

REPORT DOCUMENTATION PAGE

Form Approved
OMB No. 0704-0188

Public reporting burden for this collection of information is estimated to average 1 hour per response, including the time for reviewing instructions, searching existing data sources, gathering and maintaining the data needed, and completing and reviewing this collection of information. Send comments regarding this burden estimate or any other aspect of this collection of information, including suggestions for reducing this burden to Department of Defense, Washington Headquarters Services, Directorate for Information Operations and Reports (0704-0188), 1215 Jefferson Davis Highway, Suite 1204, Arlington, VA 22202-4302. Respondents should be aware that notwithstanding any other provision of law, no person shall be subject to any penalty for failing to comply with a collection of information if it does not display a currently valid OMB control number. PLEASE DO NOT RETURN YOUR FORM TO THE ABOVE ADDRESS.

1. REPORT DATE (DD-MM-YYYY)	2. REPORT TYPE Technical Paper	3. DATES COVERED (From - To)
------------------------------------	--	-------------------------------------

4. TITLE AND SUBTITLE	5a. CONTRACT NUMBER
	5b. GRANT NUMBER
	5c. PROGRAM ELEMENT NUMBER 62500F

6. AUTHOR(S)	5d. PROJECT NUMBER 2308
	5e. TASK NUMBER M4S7
	5f. WORK UNIT NUMBER 345382

7. PERFORMING ORGANIZATION NAME(S) AND ADDRESS(ES)	8. PERFORMING ORGANIZATION REPORT
---	--

9. SPONSORING / MONITORING AGENCY NAME(S) AND ADDRESS(ES) Air Force Research Laboratory (AFMC) AFRL/PRS 5 Pollux Drive. Edwards AFB CA 93524-7048	10. SPONSOR/MONITOR'S ACRONYM(S)
	11. SPONSOR/MONITOR'S NUMBER(S)

12. DISTRIBUTION / AVAILABILITY STATEMENT Approved for public release; distribution unlimited.
--

13. SUPPLEMENTARY NOTES See attached 13 papers, all with the information on this page.
--

14. ABSTRACT
15. SUBJECT TERMS

16. SECURITY CLASSIFICATION OF:			17. LIMITATION OF ABSTRACT A	18. NUMBER OF PAGES	19a. NAME OF RESPONSIBLE PERSON Kenette Gfeller
a. REPORT Unclassified	b. ABSTRACT Unclassified	c. THIS PAGE Unclassified			19b. TELEPHONE NUMBER (include area code) (661) 275-5016



AIAA-96-3185

**Comparisons of Hydrogen Atom Measurements
in an Arcjet Plume with DSMC Predictions**

Ingrid J. Wysong, Jeffrey A. Pobst
Hughes STX
Propulsion Directorate
OL-AC Phillips Laboratory
Edwards AFB, CA

Iain D. Boyd
School of Mechanical and Aerospace Engineering
Cornell University
Ithaca, NY

**32nd AIAA/ASME/SAE/ASEE
Joint Propulsion Conference
July 1-3, 1996 / Lake Buena Vista, FL**

Comparisons of Hydrogen Atom Measurements in an Arcjet Plume with DSMC Predictions

Ingrid J. Wysong* and Jeffrey A. Pobst**
Hughes STX
Phillips Laboratory, Propulsion Directorate
Edwards AFB, CA

Iain D. Boyd†
School of Mechanical and Aerospace Engineering
Cornell University
Ithaca, NY

Abstract

We present comparisons between hydrogen atom number density, velocity, and temperature measurements with DSMC predictions at nozzle exit for two power levels of a hydrogen arcjet thruster: 1.34 kW and 800 W. Comparisons between model and experiment are also presented in two downstream plume regions. Atomic density peaks at each power are not seen to vary substantially while velocity and temperature maximums decrease with lower power operation. Changes in profile shapes are noticed at the different powers and similar profile changes are also observed in the model predictions. Differences in overall magnitude are observed at some locations between measured data and predicted results, but in general the model matches the measured data quite well.

Introduction

Arcjet thruster computational models have begun to reach a level of maturity where new advanced thruster designs may soon be based upon model predictions. Concurrently, there is interest in the development of a new arcjet thruster class, designed for operation at powers lower than 1000 watts. In order to design thrusters of this type from model predictions, the scaling of present thruster predictions into this lower power region must be explored.

As thruster designs become physically smaller, changes in the energy loss mechanisms of the nonequilibrium gas flow are expected. The direct simulation Monte Carlo (DSMC) method, while computationally intensive, provides a direct simulation of collision and plasma behavior and is therefore able to model gas flows with high degrees of nonequilibrium. The nonequilibrium of the gas

becomes even greater in the plume expansion region, which is critical for determining spacecraft interaction and contamination issues. A DSMC model optimized for arcjet prediction is currently under development at Cornell University.¹

Recently, measurements of atomic hydrogen number density, ground state temperature, and species velocity were taken in the plume of a one kilowatt class arcjet thruster using a two-photon laser induced fluorescence (2PLIF) technique.^{2,3} Comparisons between the density measurements and several arcjet computational models inferred that the models tended to predict significantly lower atomic number densities than was measured with the 2PLIF technique.

Additionally, molecular dissociation fraction at the center of the nozzle exit, as determined by a combination of the 2PLIF work and molecular density data from Raman spectroscopy,⁴ was found to be higher than that predicted by the models perhaps indicating more frozen flow losses than previously thought.

Frozen flow losses, already significant in 1 kW arcjets may be more of a dominant factor in limiting the attainable efficiency of lower power arcjet thrusters. Investigation into low power arcjet operation and how it may differ from higher power operation is therefore warranted including a

* Principal Scientist, Member AIAA

** Senior Scientist, Member AIAA

† Associate Professor, Member AIAA

Copyright © 1996 American Institute of Aeronautics and Astronautics. All rights reserved. No copyright is asserted in the United States under Title 17, U.S.C. The Government has a royalty free license to exercise all rights under the copyright claimed herein for Government purposes. All other rights are reserved by copyright owner. This paper is declared a work of the U.S. Government and is not subject to copyright protection in the United States.

20050815 023

comparison of how the models predict operation at these lower powers.

Experimental Technique and Analysis

The experimental technique used to measure atomic densities and temperatures has been described in previous papers.^{2,3} Two-photon laser-induced fluorescence (2PLIF) at 205 nm is used to probe ground state hydrogen atoms at various points in the arcjet plume. Through measured Doppler shifts, Doppler widths and calibrated intensities of the resulting fluorescence, velocity, temperature and number density may be inferred.

Since any propellant gas is opaque for the VUV radiation required for single-photon excitation of ground state atoms, 2PLIF at correspondingly longer wavelengths is preferred. The diagnostic technique, which has been developed primarily for use in flames,^{5,6,7} uses two photons at 205 nm to promote the atoms from the $n=1$ to the $n=3$ electronic state (the $L\beta$ transition). Subsequent 3-2 fluorescence is observed (the $H\alpha$ transition), as shown in the energy level diagram in Figure 1.

The apparatus is shown schematically in Figure 2. The laser is a pulsed dye laser pumped by a Nd:YAG with a repetition rate of 10 Hz and a pulse width of 6 ns. The dye laser output at 615 nm is frequency tripled to achieve about 0.5 mJ per pulse at 205 nm. A mirror turns about 80% of the beam toward the arcjet chamber through a variable attenuator placed in the beam, the remaining 20% of beam energy is directed toward a microwave-discharge source of atomic hydrogen.

The laser beam and optics remain fixed, while the arcjet is mounted on a motion control x, y, z stage to translate it for probing different regions of the plume. Detection of the fluorescence takes place with a spectrally filtered and temporally gated photomultiplier tube collecting light from the side of the chamber. A calibration cell with microwave discharge source outside the chamber provides a wavelength reference during laser spectral tuning.

For axial velocity measurements, the beam is sent directly down the axis of the arcjet flow (Path 1) and is focused with a telescope lens configuration (not shown) outside the chamber with a focal length on the order of 2 m. For radial measurements, the unfocused beam can be sent to a turning prism inside the chamber located underneath the arcjet (Path 2), directed to pass vertically through the plume, and

focused by a 200 mm lens. For the work presented here, all data was taken down the axis of the arcjet flow. Radial data from a 1.34 kW arcjet plume along with a more detailed experimental setup description is presented in previous work.³

The procedure for obtaining absolute number density values from the measured fluorescence intensity is based on a method reported by Meier et al.^{7,8} and Tserepi et al.⁹ Prior to taking relative number density and lifetime data in the lit arcjet plume, the arcjet is translated away from the collection volume with the chamber open and a second calibration cell is placed in the detection volume with the laser beam passing through it. The LIF signal and lifetime is measured for the hydrogen atoms present in the cell. Atoms are present due to the flow of hydrogen gas through a microwave discharge prior to entering the cell. Since the laser beam, detection optics and electronics have remained the same, the LIF from the arcjet and from the cell will have the same proportionality to absolute number density after correcting for any differences in quenching and window losses:

$$N_H^A = \frac{S^A}{S^C} \cdot N_H^C \cdot C_Q$$

S^A and S^C are the signal sizes (integrated over the entire spectral width) from the arcjet and the cell, N_H^A and N_H^C are the absolute number densities of atomic hydrogen in the arcjet and the cell, and C_Q is the scaling factor for the difference in quenching. C_Q is given by the ratio of fluorescence decay rate in the arcjet to that in the calibration cell.

The absolute number density of hydrogen atoms in the discharge cell is obtained using a standard chemical titration method. A schematic of the calibration cell used for this method is shown in Figure 3. The cell is made out of glass tubing and is approximately 30 cm (12 in.) long and 5 cm (2 in.) in diameter. Important to the design of the cell is the long drift tube area with a Teflon tubing liner to reduce gas/wall interactions. This drift tube allows complete mixing of the titration gas and the gas of interest. In this case, the titration gas is NO_2 and H is the gas to be calibrated.

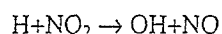
The hydrogen (with a helium carrier gas) enters the drift tube area near one end after passing through a microwave discharge. A dilute mixture of NO_2 in helium is added to the flow through a long thin tube and enters the larger drift tube region at a location past the point where the hydrogen has entered. This

reduces the amount of NO₂ that might diffuse upstream and enter the microwave discharge.

Placing the end of the tube somewhat closer to the collection volume than the microwave discharge leads to a better response of signal to NO₂ addition. This is believed to be due to reduced NO₂ upstream diffusion which, if allowed to become significant, appears to influence the number of H atoms produced in the microwave discharge. Placing the end of the tube five or six inches downstream of the entrance of the atomic hydrogen appears to prevent this effect for the following flow rates.

The NO₂ reacts rapidly with hydrogen atoms when the two are completely mixed in the large drift tube volume. The calibration involved flowing 1 slpm of a 2% hydrogen in helium mixture and then the addition of 2% NO₂ in helium until the signal decreased, typically at about .08 slpm of NO₂/He. A small vacuum pump brought the cell pressure down to 950 Pa (7.2 Torr) during gas flow.

The LIF signal decreases until it is gone at the point where the partial pressure of added NO₂ is equal to the partial pressure of hydrogen atoms in the cell. Control of the amount of NO₂ added allows the determination of the amount of hydrogen atoms present in the calibration cell. Figure 4 shows data from one calibration run. The NO₂ concentration at the x intercept is equal to the concentration of atomic hydrogen present as each hydrogen atom is reacted away for each NO₂ molecule added in the fast reaction:



The large amount of buffer gas and low amount of H significantly reduce possible secondary reactions, making them negligible for the purposes of this experiment. Calibration took place just prior to each arcjet firing.

All thruster data were taken on a 1-kW-class arcjet designed by NASA Lewis Research Center.¹⁰ The cathode gap was set to 0.07". The arcjet operated at either 134V, 10A (1.34 kW - a control condition similar to previous results) or at 154V, 5.2A (800 W - the lower power condition examined in this work) both on a hydrogen gas flow of 13.1 mg/s (8.74 slpm) at an operating chamber pressure of 6 Pa (45 mTorr).

A voltage-current curve of our arcjet, was shown in a previous publication² and was verified prior to taking the results for this work. The hydrogen flow

controller for the arcjet as well as the flow meters for the discharge cell were calibrated using a wet test meter.

Figure 5 shows a sample spectral scan of the hydrogen atom profile from the arcjet and from the discharge cell, taken with an axial laser beam. Each profile is fit to a Gaussian shape using a Levenberg-Marquardt least squares fit.¹¹ The wavelength shift of the two centers yields the axial velocity, the width of each Gaussian yields the temperature, and the integrated fluorescence intensity is compared to the calibration cell described above to determine a number density value.

A number of possible uncertainties enter into this analysis. A focused pulsed laser beam creates a very high instantaneous energy density, which is needed to excite the two-photon transition, but also may induce other non-linear processes such as multiphoton ionization (MPI), partial saturation of the transition (possible, even though the two-photon absorption cross section is very small), and amplified spontaneous emission (ASE). Since the transition of interest is a two photon one, the unsaturated LIF signal desired is proportional to laser power squared. A laser power dependence study is performed to verify that the laser power is attenuated enough to remain in a region of fluorescence proportional to laser power squared.

Another mechanism which can cause misinterpretation of the fluorescence is Stark broadening. Based upon previous analysis,³ the maximum Stark effect in the center of the nozzle may cause us to overpredict temperatures by 7% and densities by less than 3%.

Additionally, a small amount of line broadening is caused by the linewidth of the dye laser beam which, unlike that of continuous wavelength ring dye lasers, is non-negligible compared with the atomic linewidth. Studies have shown that the laser has a width of 0.28 cm⁻¹ or 0.012 Å at 205 nm. The effect of the laser width is taken into account using the following relation:¹²

$$(\Delta v)^2 = (\Delta v_D)^2 + 2(\Delta v_l)^2$$

where Δv_D is the true Doppler width of the line (in cm⁻¹), Δv_l is the width of the laser, Δv is the measured transition width, and the factor of two is due to the two-photon probe method.

Velocity is measured by observing the Doppler shift of the absorption line and determining the velocity relative to the incoming photons responsible for the shift.

$$v = \frac{\Delta\lambda}{\lambda_0} c$$

where v is the velocity, $\Delta\lambda$ is the wavelength shift, λ_0 is the zero velocity line center, and c is the speed of light. Determining the line center of a profile with the fitting process discussed earlier is relatively simple and quite accurate. The uncertainty from the data analysis is less than the symbol size of the data shown in velocity figures.

Low signal to noise of the fluorescence (when low laser power is used to prevent non-linear effects) makes measurement of the Doppler width difficult, especially at the edges of the plume, though Doppler shift measurements are less affected. Temperature is based upon the square of the measured Doppler width and can be written in terms of width in the following manner.¹³

$$\delta\lambda = 7.16 \times 10^{-7} \lambda_0 \sqrt{\frac{T}{M}}$$

where $\delta\lambda$ is the linewidth due to Doppler broadening, λ_0 is the line center, M is the molar mass of the gas, and T is the translational temperature. The constant in the equation is based upon the values of the speed of light and the molecular gas constant.

Substantially greater uncertainty is associated with temperature than with velocity due to the square relationship between temperature and width. The uncertainty due to scatter can be seen in the temperature plots, which include data from several different days.

Density measurements can be made by integrating the fluorescence for each transition and comparing the area to the calibrated fluorescence taken previously. As described above, a calibration cell is placed in the test chamber at the same optical location as where the arcjet is when it fires. Collisional quenching is present in the arcjet environment and variations in quenching in the plume as well as differences between the arcjet and the calibration cell must be accounted for. This is accomplished through measurements of fluorescence lifetime decay at each location where density measurements are taken in the plume. Fluorescence decay is also measured in the density calibration cell. The traces are fitted to an

exponential and the $1/e$ time of each is compared. This allows determination of the quenching effect and what compensation is required to relate the plume fluorescence to that measured in the calibration cell.

Numerical Method

The direct simulation Monte Carlo method (DSMC) uses the motions and collisions of particles to perform a direct simulation of nonequilibrium gas dynamics. Each particle has coordinates in physical space, three velocity components, and internal energies. A computational grid is employed to group together particles that are likely to collide. Collision selection is based on a probability model developed from basic concepts in kinetic theory. The method is widely used for rarefied nonequilibrium conditions and finds application in hypersonics, materials processing, and micro-machine flows.

The extension of the technique for application to arcjet flows is described in detail by Boyd.¹ This required development of a number of new physical models. Arcjets are characterized by high temperatures (as high as 30,000 K) which give rise to strongly ionized flows (as much as 30% ionized). In terms of intermolecular collisions, mechanisms must be included in the numerical model to account for: (1) momentum transfer; (2) rotational excitation; (3) vibrational excitation; (4) dissociation/recombination; and (5) ionization/recombination. The relatively high level of ionization requires modeling of plasma effects at some level.

For a hydrogen arcjet, the four main species present are H₂, H, H⁺, and e. In general, the most important collision types that determine the arcjet flow field are H₂-H₂, H₂-H, H-H, H₂-e, and H-e. In the present work, the momentum transfer cross-sections for the first three collision types are obtained from the work of Vanderslice et al.¹⁴ in which collision integrals were tabulated for the temperature range of 1,000 to 15,000 K. The cross-sections for the H₂-e collision is determined using the experimental data of Crompton and Sutton.¹⁵ The cross-section for the H-e collision is determined using the simple analytical expression given by Yos.¹⁶ The level of agreement between the models used in the DSMC code and the original sources is very good with the exception of the H₂-e collision. Other cross-sections are much less important and are assigned values such that the results of hydrogen atoms are used for hydrogen ions. For example, the cross-sections for H₂-H collisions are also used for H₂-H⁺ collisions. While this results in some lack of accuracy, it is expected that the effect

will be small as these collisions are relatively infrequent.

Molecular hydrogen is an interesting diatomic molecule in that it has relatively large values for the characteristic temperatures of rotation and vibration. This results in long relaxation times for these modes. Previously, a rate model for determining the probability of translational-rotational energy transfer for hydrogen at low temperatures was developed and verified.¹⁷ This same model is employed again here although it is recognized that it may be inaccurate at the very high temperatures encountered in the arcjet. The probability of vibrational energy exchange employs the familiar Landau-Teller relaxation time with parameters obtained experimentally by Kiefer.¹⁸ Once again it is recognized that this approach may be inaccurate at the very high temperatures found in the arcjet. There are only two chemical reactions implemented in the present study. They are dissociation of molecular hydrogen and ionization of atomic hydrogen. The rate coefficients are obtained from Refs. [19] and [20].

A very simple scheme is employed to simulate electric field effects. The electrons are constrained to move through the flow field with the average ion velocity in each cell. This ensures charge neutrality, but obviously omits the charge field effects. A second important plasma effect that is included in the DSMC simulation is ohmic heating. This is an important source of energy that results from the current represented by the flux of charged species through the thruster. Using standard plasma physics theory, a source of energy is computed in each cell of the simulation due to ohmic heating. This energy is added to the charged particles in each cell in each iteration of the calculation. The scheme is described in detail in Ref. [1].

The collision and plasma models are implemented in an existing DSMC code that is designed for efficient performance on vector supercomputers.²¹ The DSMC computations are begun at a location downstream of the nozzle throat. The initial profiles of flow properties are obtained from continuum simulations provided by the code of Butler.²² The interaction of the gas with the wall of the nozzle is assumed to be diffuse with full energy accommodation to the wall temperature profile obtained from the continuum simulation. Charged species are neutralized upon contact with the wall. The computations extend through the nozzle exit plane to a distance of 30mm from the thruster along

the axis. Expansion is assumed to occur into a perfect vacuum.

The grids employed typically consist of 500 by 55 cells. Due to the wide dynamic range in density for these flows, the cells are adapted to the local mean free path, and the time step in each cell is scaled by the local mean time between collisions. Despite the time step variation, the transient phase of the simulation remains long. Typically, it requires at least 15,000 iterations before steady state is reached. Macroscopic results are then obtained by sampling properties over a further 10,000 time steps. At steady state, there are at least 300,000 particles present in the simulation.

Results and Discussion

Measurements are made at 1.34 kW and at 800 Watts arcjet power. Both thruster configurations include mass flow of 13.1 mg/s hydrogen propellant and identical cathode spacings.

Figures 6-11 show nozzle exit atomic hydrogen properties at both 1.34 kW and at 800 W powers. The figures are grouped such that density, velocity, and temperature profiles may be compared side by side with the higher power case on the left and the lower power case on the right.

Reduction of the power by 40% did not appear to significantly impact the number density of atoms at the center of nozzle exit. Both atomic hydrogen density peaks appear to be around $1 \times 10^{16} \text{ cm}^{-3}$ and are maximum at the center of the exit plane. The 800 watt profile in Figure 7, however, appears slightly more peaked than the 1.34 kW profile in Figure 6, falling off an order of magnitude in density within 3.5 mm of center, while the higher power case takes about 4.5 mm to drop to $1 \times 10^{15} \text{ cm}^{-3}$.

Note that the model number density predictions both predict lower values than what was measured, but like the data do not show marked number density changes with changes in power. The profile shape change observed in the experimental data between the two power cases is directly predicted by the model with the more flat profile predicted in the high power case and the more peaked profile shown in the lower power case.

Comparing the velocity profiles in Figures 8 & 9, the 40% decrease in power for a constant flow rate appears to have led to a 15% decrease in maximum nozzle exit atomic hydrogen velocity and about a

25% to 30% decrease in velocity at the edges of the velocity distribution. The model prediction for both cases is quite close to the measured velocities predicting somewhat lower velocities in the higher power case and quite closely matching the data observed in the 800 watt plume. For the 800 W case, the model predicts small increases in velocity near the outer edges of the nozzle walls. While this is not directly observed in the velocity data, the features would be well within the observed velocity scatter and could be present.

The temperature distributions at nozzle exit are hard to accurately interpret using this technique due to the difficulty in ascertaining accurate Doppler widths. Comparing the two power cases in Figures 10 & 11, a overall decrease in average temperature can be seen with decrease in power, though the scatter would make a quantitative measure of the decrease tenuous.

The DSMC model predicts a peak temperature of similar magnitude to that experimentally observed, though the predicted distribution appears to drop in temperature with radius faster than the observed data does. The scatter in the experimental data is significant enough that it is not able to corroborate the predicted higher temperatures as the radial position approaches the nozzle walls. The model for the 800W case appears to underpredict the measured temperature but the shape of the profile follows the data as well as can be discerned in the scatter.

The high temperature environment of the arcjet nozzle exit often makes the use of diagnostic probes or sensors difficult or inappropriate near or on the thruster. Because of this, many optical diagnostics have been conducted in the arcjet plume region in the laboratory and ground- or space-based remote observation of arcjet plumes are even being considered for operational flight systems.²³

Understanding the behavior of the accessible arcjet plume and how it relates to internal arcjet operation is therefore desirable. The DSMC computational approach is uniquely suited to modeling the plume environment from the arcjet nozzle to the plume region and the following figures explore physical quantities at two locations in the plume: a downstream radial distribution 10 mm from nozzle exit and an axial distribution along the centerline from the nozzle to 30mm downstream.

Figures 12-17 show radial distributions about the nozzle centerline 10mm downstream of the nozzle exit. Again, the figures are grouped by physical

property (density, velocity, and temperature) and by power (1.34 kW and 800 W). Both experimental data and the DSMC prediction (solid line) are shown in each figure. Additionally, a DSMC prediction is given with the result normalized to the experimental data at the nozzle exit center (dashed line). This provides a comparison of DSMC prediction in the plume region assuming that the model and the data more closely agreed at the center of the arcjet nozzle exit. The prediction of change at a location in the plume relative to the nozzle exit conditions are thus shown in addition to the absolute predictions that take processes inside the arcjet into account.

Density distributions measured 10 mm downstream of the nozzle exit are shown in Figures 12 & 13 and appear to be slightly affected by the change in power. The density maximum in the center of the distribution drops from an average of about $2.4 \times 10^{15} \text{ cm}^{-3}$ at 1.34 kW to an average of about $1.7 \times 10^{15} \text{ cm}^{-3}$ at 800 W, though the scatter and sample size make a conclusion on power effect on peak density uncertain. At 5mm from center, the density does appear to drop as power is decreased from about $6 \times 10^{14} \text{ cm}^{-3}$ to $4 \times 10^{14} \text{ cm}^{-3}$, a decrease of over 30%, similar to what was observed at nozzle exit.

The model density predictions at 10mm downstream appear significantly lower than the measured values, but are extremely close in trend and shape. The rate of decrease from the center to the wings matches the measured data almost exactly. The overall magnitude difference already observed at nozzle exit has been compensated for in the dashed prediction and for the high power case the data and normalized prediction match almost exactly. The 800 W prediction appears to predict values lower than the data, but not by as much as the normalization factor, which when applied, causes the normalized DSMC profile to predict higher densities than observed.

The drop in peak atomic hydrogen velocity as power is decreased is almost identical to the drop observed at nozzle exit (from 13 km/s to under 11 km/s), but the distribution is substantially wider at 10 mm downstream (see Figures 14 & 15). The profile at 1.34 kW appears to drop to about 8 km/s at 10 mm from centerline and 6 km/s at 800 W. This is also a 25% decrease at the wings of the distribution similar to what was seen at the nozzle exit. The velocity profiles from the DSMC model again show slightly lower predicted velocities that almost exactly match up with the data when normalized to the nozzle exit peak velocity. It would appear that for velocity, the

change between nozzle exit and 10 mm downstream predicted by the model matches exactly the change observed in the experimental data.

The temperature profiles shown in Figures 16 & 17 are significantly different at 10 mm downstream than what was observed at the nozzle exit in Figures 10 & 11. The profiles of both powers are substantially more flat downstream and while noisy, both exhibit average temperatures of around 700 K to 800 K at either of the arcjet powers. The DSMC code, however, predicts, strong variations in temperature at the two different powers with a more peaked profile at the higher power and a more flat profile at 800 W. The model prediction normalized to the nozzle exit data does not appear to lead to better agreement between the predictions and the experimental data at this plume location.

Examination of the plume expansion along the centerline of the thruster axis takes place in Figures 18 through 23. Again, 1.34 kW operation is shown for density, velocity, and temperature in the even figures on the left, and 800 W counterparts are shown in the odd figures on the right.

Density for both powers is observed to drop exponentially (somewhat linear on a semi-log plot) though the decrease is slightly faster in Figure 18 for 1.34 kW than in Figure 19 for 800W. Noticeably different is the scatter observed at the different powers. The density at the higher power was not as repeatable day to day as was observed at 800 W operation. Though the signal to noise ratio is much better at the lower power arcjet operating condition, no explanation seems completely viable at this point to justify the differences in observed scatter. Note that at the chamber background pressure of 6 Pascals (45 mTorr), no discontinuities in density that would indicate a shock formation are observed in the atomic species density.

The Monte Carlo model predictions for the centerline densities indicate similar decreases in density with lower predicted magnitudes. When normalized with the nozzle exit and plotted using the dashed line, the trend for the 1.34 kW case matches the data well, perhaps predicting slightly higher densities in the far plume. The 800 W case also predicts lower densities than measured, but the normalized slope appears to decrease in density less rapidly than the experimental data indicates.

Figures 20 & 21 indicate that no significant perturbations to velocity are taking place due to

vacuum chamber back pressure interaction with the expansion at these operating pressures. Both velocity profiles show essentially constant velocity consistent with the centerline values previously seen at nozzle exit and at 10 mm downstream. The model predicts that at these pressures the velocities would remain constant as well, and though lower velocities are predicted, normalization, as would be expected, leads to very close match between model and experiment. The atoms in the plume along the centerline appear to expand as an undisturbed beam of particles.

Decreases in temperature from nozzle exit into the plume are observed in Figures 22 & 23. In each figure, temperatures decrease with position from the observed nozzle exit values to somewhat constant downstream values of 700K to 800K. The scatter in the lower power case is again significantly less than that observed in the higher power case. Model predictions for temperature along the centerline exhibit similar decreases. Different from the density case, the temperature predictions appear to predict lower temperatures than what the measured values indicate. Normalization of the model results lead the trends to match well for the first 10 mm and begin to diverge as the data is compared farther out in the plume.

Conclusions

Two photon laser induced fluorescence has been successfully used on various regions of an arcjet plume at both 1.34 kW and 800 W operation at a constant flow rate. Atomic hydrogen ground state densities, velocities, and temperatures have been measured at nozzle exit, 10 mm downstream of nozzle exit, and along the centerline from nozzle exit to 30 mm downstream.

Comparisons between measured data profiles at different powers demonstrate that velocity and temperature magnitudes appear to be more affected by arcjet power level than density peak values. This constant peak value of density implies a higher fraction of energy lost in frozen flow losses for the lower power case as a similar amount of energy is required to dissociate the molecules as in the higher power case. Overall density profile shapes also are observed to change as power is varied becoming more peaked in the center at lower powers. Centerline trends in these parameters do not appear to significantly change with power.

An advanced Direct Simulation Monte Carlo computational code has been optimized for use in the arcjet plasma environment including collisional,

chemical, and plasma terms to account for the processes taking place in the high temperature environment of arcjet operation. The addition of ohmic heating in the vectorized plasma module marks a significant step in the development of the code.

Comparisons between the model and experimental measurements are generally quite good, with profile trends in data and model matching for most cases. Overall magnitude differences, especially in nozzle exit number density, have yet to be fully reconciled and may be the subject of further investigation. Model predictions, through normalization with respect to the nozzle exit data, appear to describe the plume expansion extremely well, leading to the conclusion that the model appears to be mature with respect to relating plume quantities back to the nozzle exit.

Acknowledgments

The experimental research is supported by the Air Force Office of Scientific Research (AFOSR) and the Phillips Laboratory. The modeling effort at Cornell University is supported by AFOSR grant F49620-94-1-0328. Dr. Mitat A. Birkan is the AFOSR technical monitor for both efforts.

References

1. Boyd, I. D., "Monte Carlo Simulation of Nonequilibrium Flow In Low Power Hydrogen Arcjets," AIAA Paper 96-2022, 27th Fluid Dynamics Conference, New Orleans, LA, June 1996.
2. Pobst, J. A., Wysong, I. W., and Spores, R. A., "Laser Induced Fluorescence of Ground State Hydrogen Atoms at Nozzle Exit of an Arcjet Thruster," IEPC-95-28, 24th International Electric Propulsion Conference, Moscow, Russia, September 19-23, 1995.
3. Pobst, J. A., Wysong, I. W., and Spores, R. A., "Laser Induced Fluorescence of Ground State Hydrogen Atoms at Nozzle Exit of an Arcjet Thruster," AIAA-95-1973, 26th Plasmadynamics and Lasers Conference, San Diego, CA, 19-22 June 1995.
4. Beattie, D. R., and Cappelli, M. A., "Raman Scattering Measurements of Molecular Hydrogen in an Arcjet Thruster Plume," AIAA-95-1956, 26th AIAA Plasmadynamics and Lasers Conference, San Diego, CA, June 19-22, 1995.
5. Goldsmith, J.E.M., Miller, J.A., Anderson, R.J.M., and Williams, L.R., "Multiphoton - excited fluorescence measurements of absolute concentration profiles of atomic hydrogen in low-pressure flames," Proceedings of the 23rd Symposium (International) on Combustion, Combustion Institute, 1821 (1990).
6. Preppernau, B.L., Dolson, D.A., Gottscho, R.A., and Miller, T.A., "Temporally resolved laser diagnostic measurements of atomic hydrogen concentrations in RF plasma discharges," Plasma Chem. and Plasma Proc. 9, 157 (1989).
7. Bittner, J., Kohse-Hoinghaus, K., Meier, U., Kelm, S., and Just, T.H., "Determination of Absolute H Atom Concentrations in Low-Pressure Flames by Two-Photon Laser-Excited Fluorescence," Combustion and Flame 71, 41-50 (1988).
8. Meier, U., Kohse-Hoinghaus, K., and Just, Th., "H and O atom detection for combustion applications: study of quenching and laser photolysis effects," Chem. Phys. Lett. 126, 567 (1986); U. Meier, K. Kohse-Hoinghaus, L. Schafer, and C.-P. Klages, "Two-photon excited LIF determination of H-atom concentrations near a heated filament in a low-pressure H₂ environment," Appl. Opt. 29, 4993 (1990).
9. Tserepi, A. D., Dunlop, J. R., Preppernau, B. L., and Miller, T. A., "Absolute H-atom Concentration Profiles in Continuous and Pulsed RF Discharges," J. Appl. Phys. 72, No. 7, 2638 (1992).
10. Curran F.M., and Haag, T.W., "An Extended Life and Performance Test of a Low Power Arcjet," Paper AIAA-88-3106, 24th Joint Propulsion Conference, 1988, New York, New York.
11. Press, W. H., Flannery, B. P., Teukolsky, S. A., and Vetterling, W. T., *Numerical Recipes: The Art of Scientific Computing*, 1st ed., Cambridge Univ. Press, Cambridge, 1986.
12. Bamford, D.J., Jusinski, L.E., and Bischel, W.K., "Absolute two-photon absorption and three-photon ionization cross sections for atomic oxygen," Phys. Rev A 34, 185-198 (1986).
13. Demtröder, W., *Laser Spectroscopy, Basic Concepts and Instrumentation*, 3rd Printing, Springer-Verlag, Berlin, 1988.
14. Vanderslice, J. T., Weissman, S., Mason, E. A., and Fallon, R. J., "High-Temperature Transport Properties of Dissociating Hydrogen," Physics of Fluids, Vol. 5, 1962, pp. 155-164.
15. Crompton, R. W. and Sutton, D. J., "Experimental Investigation of the Diffusion of Slow Electrons in Nitrogen and Hydrogen," Proceedings of the Royal Society, Vol. A215, 1952, pp. 467-480.
16. Yos, J. M., "Transport Properties of Nitrogen, Hydrogen, Oxygen, and Air to 30,000K," AVCO Research and Advanced Development Technical Memorandum 63-7, 1963.
17. Boyd, I. D., Beattie, D. R., and Cappelli, M. A., "Numerical and Experimental Investigations of Low-density Supersonic Jets of Hydrogen," Journal of Fluid Mechanics, Vol. 280, 1994, pp. 41-67.
18. Kiefer, J. H., Journal of Chemical Physics, Vol. 57, 1962, p. 1938.
19. NIST Chemical Kinetics Database, Version 5.0, NIST, Gaithersburg, MD.
20. McCay, T. D. and Dexter, C. E., "Chemical Kinetic Performance Losses for a Hydrogen Laser Thermal Thruster," Journal of Spacecraft and Rockets, Vol. 24, 1987, pp. 372-376.
21. Boyd, I. D., "Vectorization of a Monte Carlo Method For Nonequilibrium Gas Dynamics," Journal of Computational Physics, Vol. 96, 1991, pp. 411-427.
22. Butler, G. W., Boyd, I. D., and Cappelli, M. A., "Nonequilibrium Flow Phenomena in Low Power Hydrogen Arcjets," AIAA-95-2819, 31st Joint Propulsion Conference and Exhibit, San Diego, CA, July 10-12, 1995.
23. J. Leduc, K.A. McFall, J.A. Pobst, D. Tilley, A. Sutton, L. Johnson, and D. Bromaghim, "Performance, Contamination, Electro-magnetic, and Optical Flight Measurement Development for the Electric Propulsion Space Experiment," Paper AIAA-96-2727, 31st Joint Propulsion Conference, Orlando, FL, July 1996.

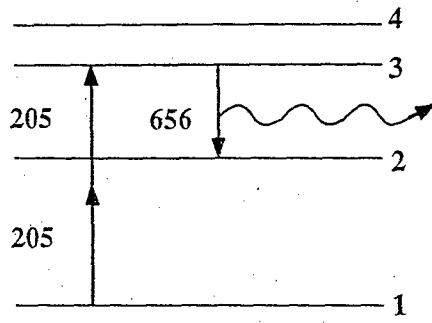


Figure 1. Energy level schematic (not to scale) of the hydrogen atom, showing the 2PLIF diagnostic technique.

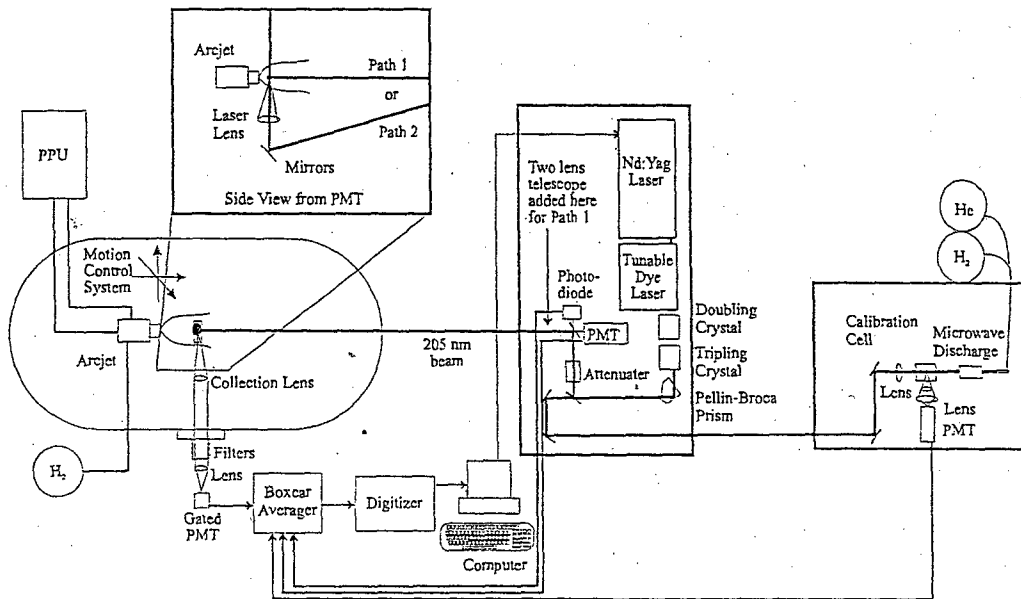


Figure 2. Experimental apparatus.

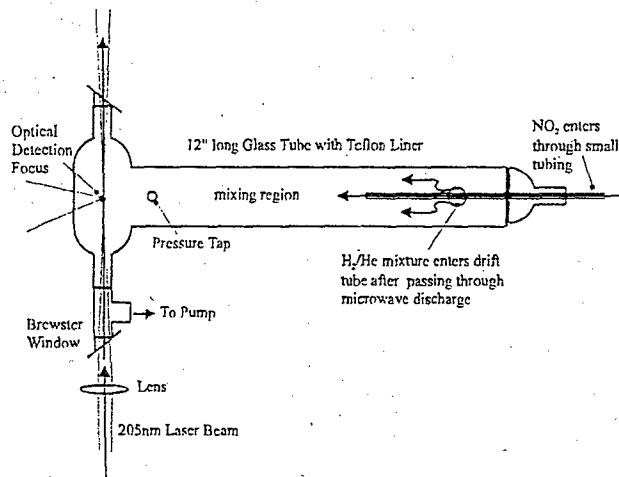


Figure 3. Calibration cell schematic for in-situ density calibration.

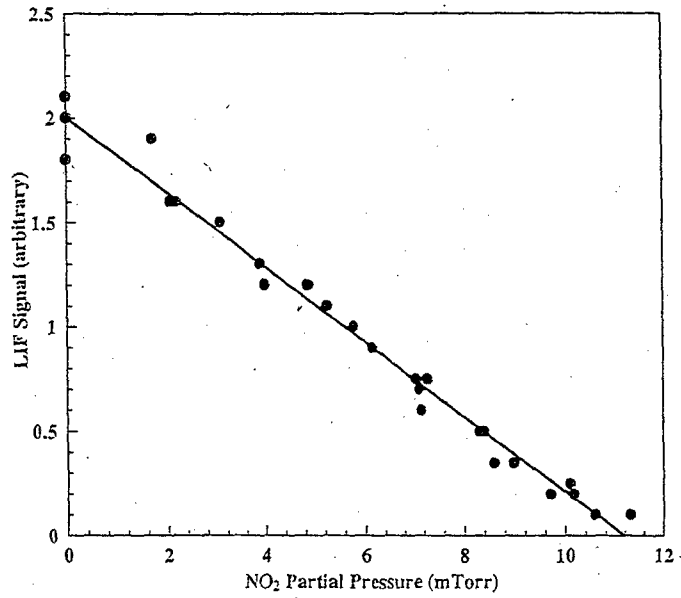


Figure 4. Determination of atomic hydrogen density and emitted signal through titration of NO₂ into calibration cell.

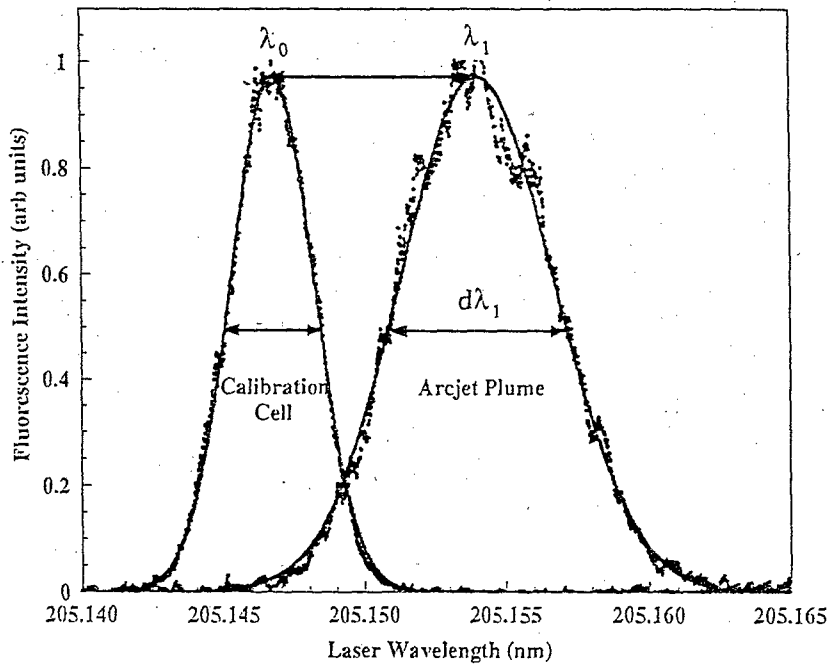
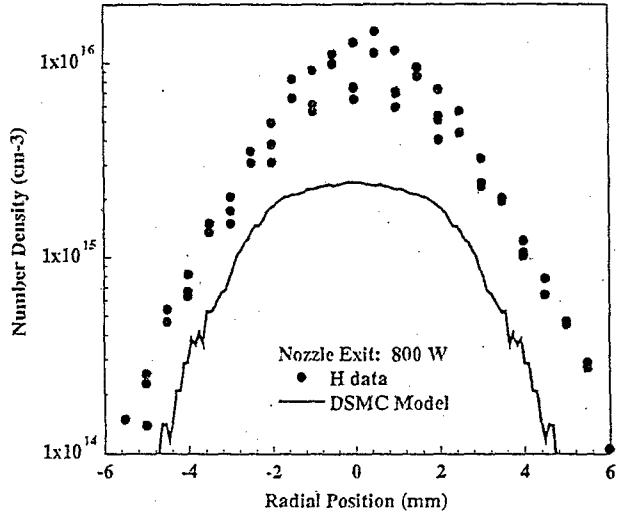
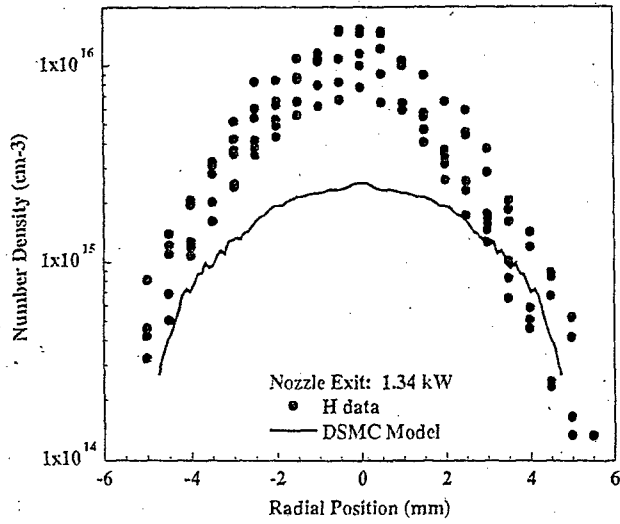
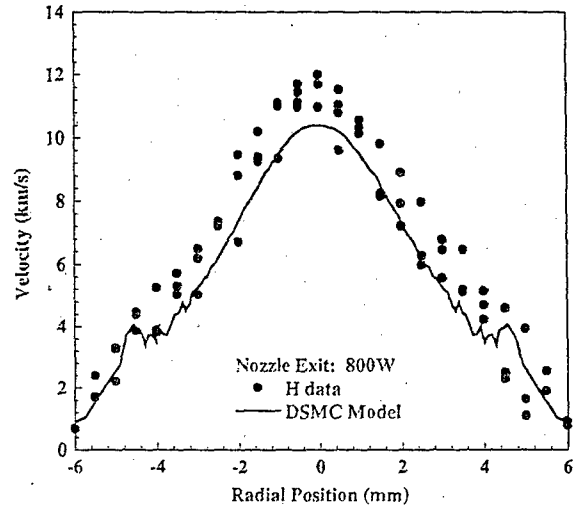
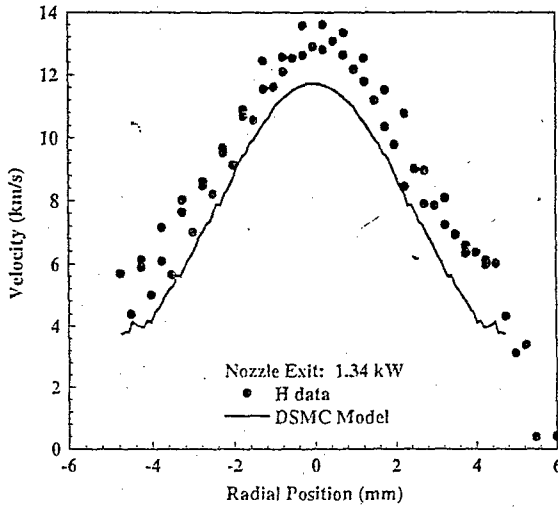


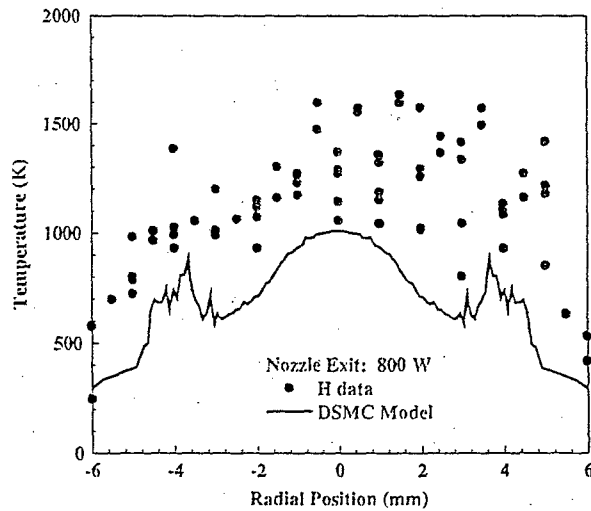
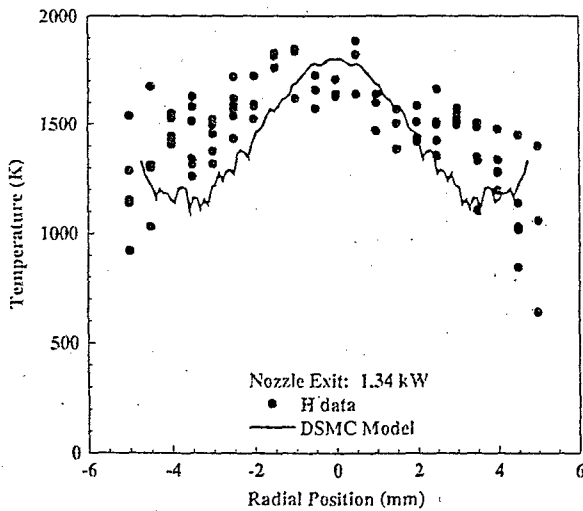
Figure 5. Sample 2PLIF spectrum of the hydrogen atom, showing the calibration signal from the discharge cell, the signal from the arcjet plume, and least-squares Gaussian curve fits for each.



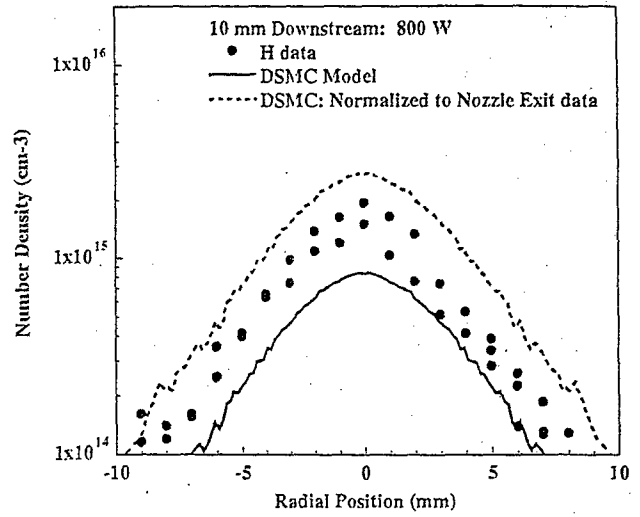
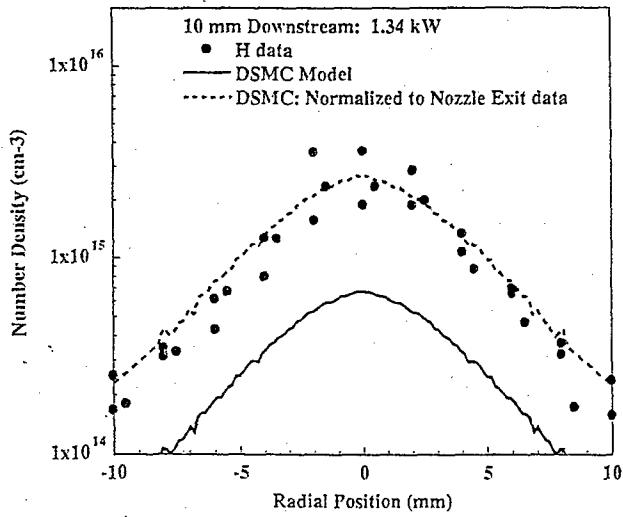
Figures 6 & 7: H density measurements and predictions at arcjet nozzle exit for 1.34 kW and 800 W



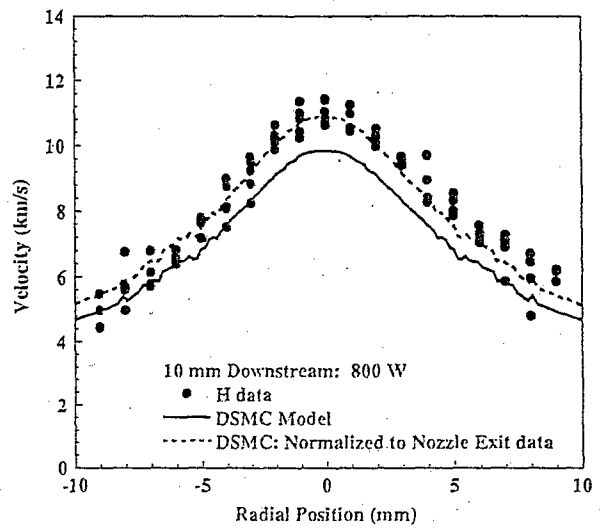
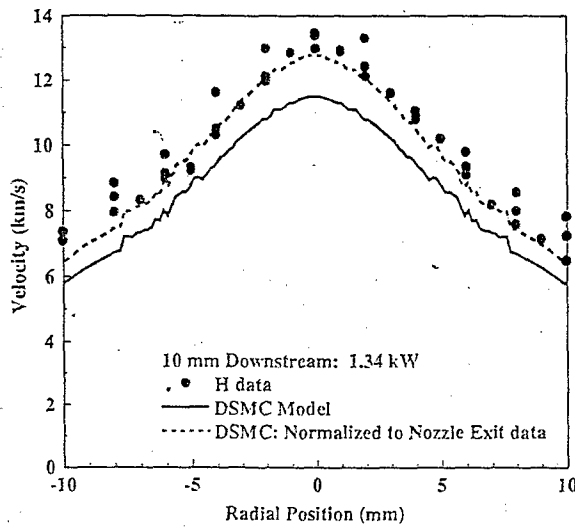
Figures 8 & 9: H velocity measurements and predictions at arcjet nozzle exit for 1.34 kW and 800 W



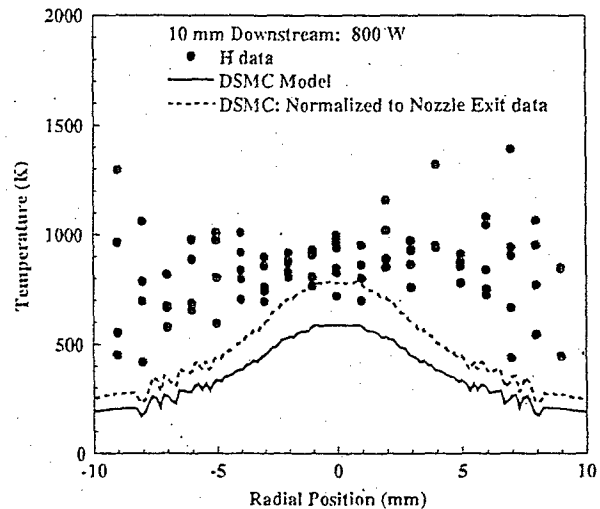
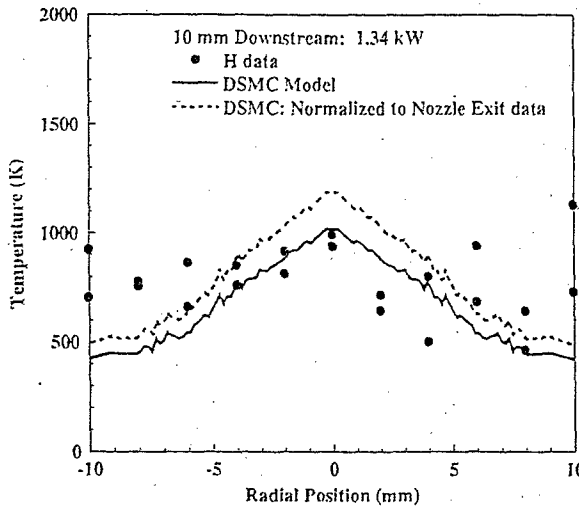
Figures 10 & 11: H temperature measurements and predictions at arcjet nozzle exit for 1.34 kW and 800 W



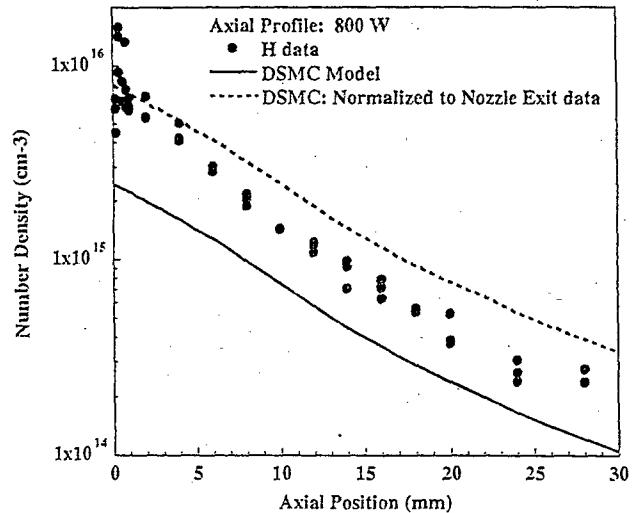
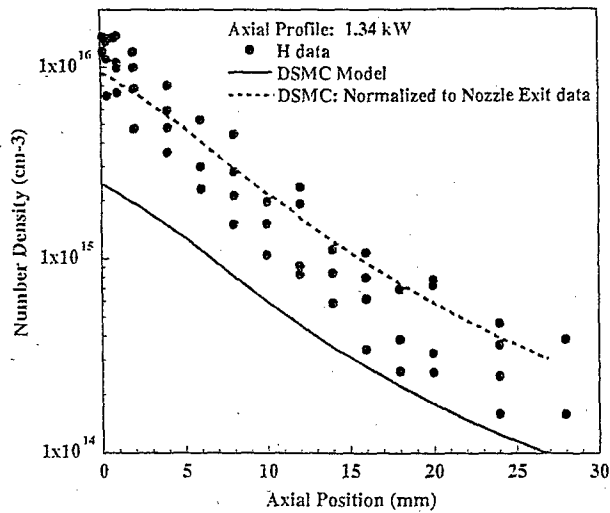
Figures 12 & 13: H density measurements, predictions, and normalized predictions 10 mm from nozzle exit.



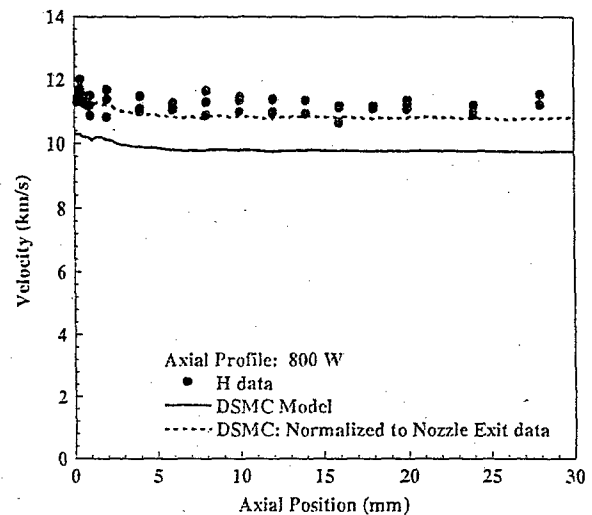
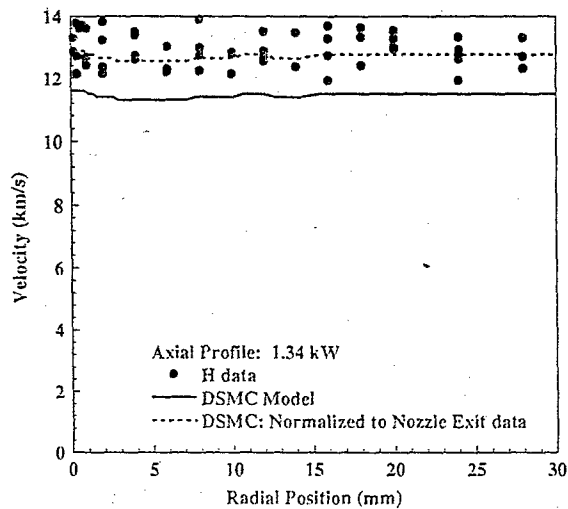
Figures 14 & 15: H velocity measurements, predictions, and normalized predictions 10 mm from nozzle exit.



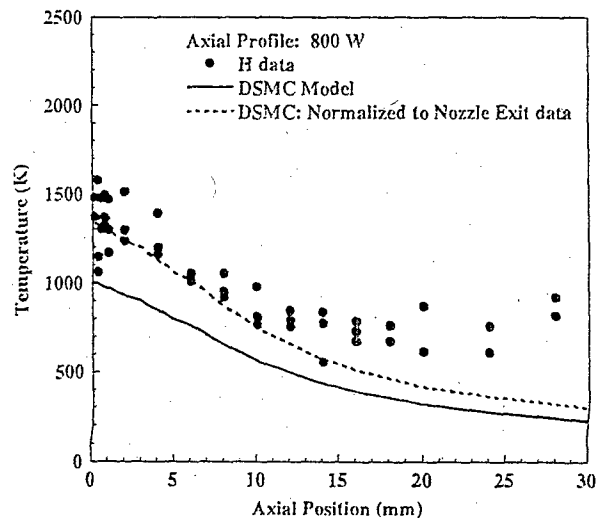
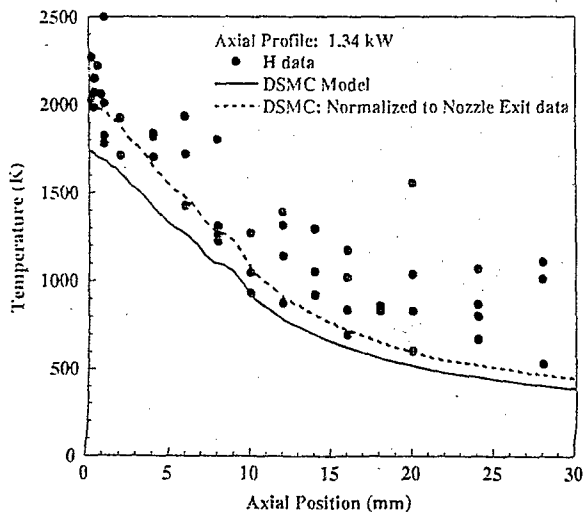
Figures 16 & 17: H temperature measurements, predictions, and normalized predictions 10 mm from nozzle exit.



Figures 18 & 19: H density measurements, predictions, and normalized predictions along the axial centerline.



Figures 20 & 21: H velocity measurements, predictions, and normalized predictions along the axial centerline.



Figures 22 & 23: H temperature measurements, predictions, and normalized predictions along the axial centerline.